Efficient Methods to Enhance the Bandwidths of Transmitarray Antennas

Mei, Peng; Cai, Yang; Zhang, Shuai

Published in:
2024 IEEE International Workshop on Antenna Technology, iWAT 2024

DOI (link to publication from Publisher):
10.1109/iWAT57102.2024.10535775

Publication date:
2024

Document Version
Accepted author manuscript, peer reviewed version

Efficient Methods to Enhance the Bandwidths of Transmitarray Antennas

Peng Mei, Yang Cai, Shuai Zhang
Antennas, Propagation and Millimeter-Wave Systems, Department of Electronic Systems, Aalborg University, Aalborg, Denmark, mei@es.aau.dk, yangc@es.aau.dk, sz@es.aau.dk

***Abstract*— This paper introduces two efficient methods to enhance the bandwidths of transmitarray antennas. For the transmitarray antenna based on resonant unit cells, two unit cells based on polarization-rotation structures are proposed to offer a 2-bit transmission phase, where the resizing unit cell is avoided to widen the bandwidth. For the lens antenna based on dielectric stubs, four unit cells are selected to offer a 2-bit transmission phase as well, to broaden the bandwidth, the effects of the oblique incidences are considered and eliminated. For the first transmitarray antenna using the proposed method, the measured 1- and 3-dB gain bandwidth is 28.0 - 37.5 GHz (29.5%) and 25.1 - 39.1 GHz (43.7%), respectively. For the second lens antenna using the corresponding proposed method, the measured 1-dB gain bandwidth is 24.8 – 30 GHz (18.9%). The proposed two methods are generalized and is also feasible for reflectarray antennas and reconfigurable intelligent surfaces.**

***Index Terms*— Transmitarray antenna, lens antenna, bandwidth enhancement, oblique incidences.**

I. INTRODUCTION

High gain and wideband millimeter-wave antennas are potentially good solutions to offer high capacity of 2-7 Gb/s to fulfill the rapid growth of mobile data traffic in point-to-point or backhauling communications [1], [2]. Transmitarray (TA) and lens antennas have attracted many interests due to their unique advantages, such as high gain, low cost, simple feeding technique and so on [3]-[6]. Generally, TA antennas suffer from narrow bandwidths due to the resonant properties of the utilized elements. However, the bandwidth limitations of such resonant elements can be improved by optimizing the element structures as reported in [3], [4], [7], [8]. One prevalent method to enhance the bandwidth of a transmitarray antenna is using the unit cells based on polarization-rotation structures to provide either continuous [9] or discrete transmission phases [10], [11]. One PR element can naturally provide two different transmission phases (with a phase difference of π) by simply rotating the middle metal layer $\pi/2$. In [11], the authors presented a PR element with cross-shaped metallic strips tilted $\pi/4$ in the middle layer to achieve a 2-bit transmission phase by varying the dimensions of the cross-shaped metallic strips. The corresponding TA antenna was fabricated and measured, revealing a 3-dB gain bandwidth of 24.1%. It should be noticed that the bandwidth the element would be shrunk when its dimensions are varied to achieve two or more transmission phases, leading to lower performance of the corresponding TA antenna. For the lens antennas implemented with dielectric stubs, the effects of oblique incidences are much more significant compared to the lens antennas implemented with planar unit cells. However, the oblique incidence effects are usually ignored in the lens antenna design since the extraction of oblique incidence effects are quite challenging.

Based on the two critical technical issues mentioned above, we introduce two efficient methods reported in my previous work [12][13] to enhance the bandwidth of transmitarray antenna implemented with polarization-rotation structures and lens antenna implemented with dielectric stubs, respectively, namely, achieving a 2-bit transmission phase without relying on resizing a single unit cell anymore for the transmitarray antenna and compensating for the effects of oblique incidences for the lens antenna. The measured results demonstrate that the 1- and 3-dB gain bandwidth is 28.0 - 37.5 GHz (29.5%) and 25.1- 39.1 GHz (43.7%), respectively, for the transmitarray antenna. while for the lens antenna, the measured 1-dB gain bandwidth can reach 24. 8 - 30 GHz (18.9%) and the gain is also enhanced.

II. METHOD TO ENHANCE THE BANDWIDTH OF TRANSMITARRAY ANTENNA

Fig. 1 presents the geometries of the proposed two elements. Each element consists of five metal layers and four substrate layers. The 1st, 3rd, and 5th metal layers are identical polarizer grids, where the 3rd metal layer is orthogonal to the 1st and 5th metal layers. The 2nd and 4th metal layers are identical polarization-rotating type metallic strips. The supporting substrates (see the green layers in Fig. 1) are Rogers 4003C with a dielectric constant of 3.55 and a loss tangent of 0.0027. The supporting substrate of the 4th metal layer is 0.508 mm thick, while the supporting substrates of the 1st, 2nd, and 3rd metal layers are 0.305 mm thick. Three bonding films (see the blue layers in Fig 1) are employed to glue different Rogers 4003C substrates tightly together. The bonding films used here are Rogers 4450F with a dielectric constant of 3.52, a loss tangent of 0.004, and a thickness of 0.202 mm. The total thickness of the element is 0.2 λ (λ is the wavelength at 30

GHz). The proposed element has the following features compared to the structure with three metal layers described in [9]-[11]: a). The polarizations of the incident and transmitted waves are the same for the proposed TA antenna by adding the two extra metal layers, while it is orthogonal for the one implemented by three metal layers structure in [9]-[11]; b). The transmission phase of the proposed element is doubled when the EM wave propagates through it since there are two identical polarization-rotating type layers (2nd and 4th metal layer). So, it is much easier to obtain to the required phase than those in [9]-[11], which also helps further broaden the bandwidth.

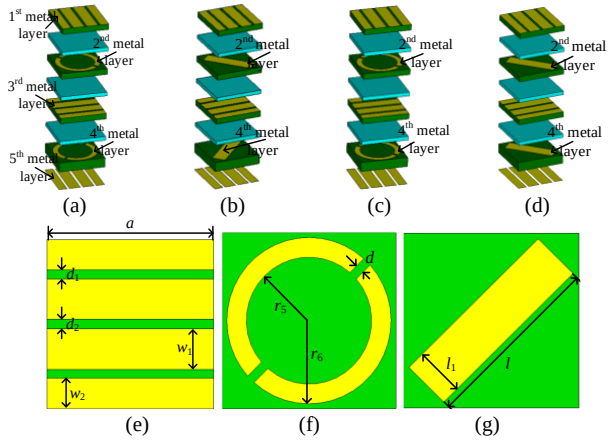

Fig. 1. Geometries of the proposed two FSS-based elements with different configurations. Expanded view of (a). Element 1 with a "**00**" transmission phase, (b). Element 2 with a "**01**" transmission phase, (c) Element 1 with a "**10**" transmission phase, and (d). Element 2 with a "**11**" transmission phase. Front view of: (e). Polarizer grid of Elements, (f). The 2nd metal layer of Element 1, and (g). The 2nd metal layer of Element 2.

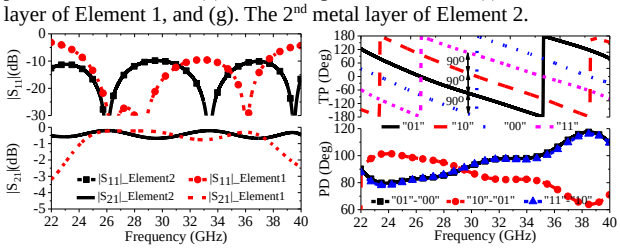

Fig. 2. S-parameters of the proposed two FSS-based elements. (a). Reflection and transmission amplitudes of S_{11} and S_{21}. (b) Transmission phases and phase differences of the two FSS-based elements (TP: transmission phase; PD: phase difference).

The expanded views of the proposed two elements are shown in Figs. 1 (a) - (d), where the split circular ring and rectangular metallic strip tilted π/4 are selected as the 2nd and 4th metal layers. The dimensions of the two elements are determined to make them operate in the 5G millimeter-wave bands and given as follows: a = 2.5 mm, d_1 = 0.13 mm, d_2 = 0.14 mm, w_1 = 0.6 mm, w_2 = 0.45 mm, d = 0.13 mm, l = 2.6 mm, l_1 = 0.7 mm, r_5 = 0.9 mm, r_6 = 1.18 mm. The proposed two elements are polarization-rotating type structures. Each element can naturally provide two transmission phases with a π phase difference by rotating one polarization-rotating metal layer by 90 deg (either 2nd or 4th metal layer in Fig. 1) with all the other dimensions fixed, while still maintaining the amplitudes of its S-parameters. Here, we fix the 2nd metal layer but rotate the 4th metal layer as shown in Figs. 1 (c) and (d). A 2-bit digital code can be used to characterize the transmission phases of the two elements as seen in Fig. 1, where the element 1 provides the transmission phases of -π and 0, and the element 2 is responsible for the transmission phases of –π/2 and π/2. As seen in Fig. 2 (a), the two elements have low insertion loss from 22 to 40 GHz. In particular, the insertion loss is less than 1dB from 24 to 38 GHz for both elements. The transmission phases of the elements with different codes are plotted in Fig. 2 (b), where a π/2 transmission phase gradient is achieved from 22 to 40 GHz. The simulated results in Fig. 2 (a) indicates that the bandwidth with low insertion loss can be significantly broadened by applying two different elements to provide a 2-bit transmission phase without resizing their dimensions.

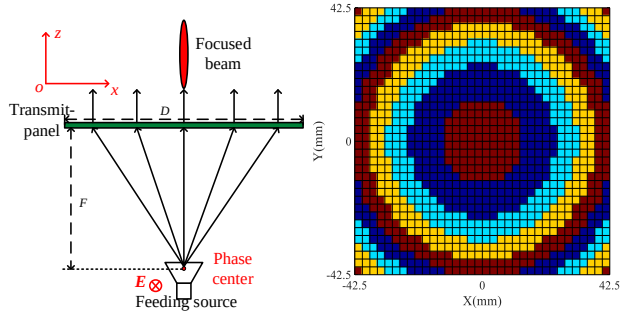

Fig. 3. (a). Schematic diagram of a TA antenna. (b). Phase distributions on the plane of the transmit-panel at 28 GHz.(■: π/2, ■: 0, ■: -π/2, ■: -π.)

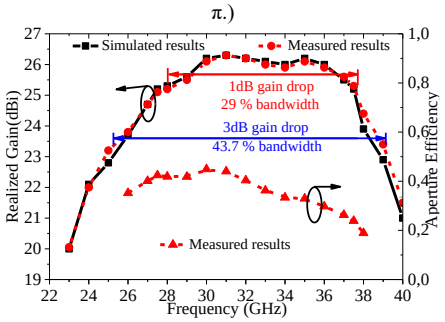

Fig. 4. Measured and simulated realized gain of the proposed TA antenna and the measured aperture efficiency.

The proposed two elements with a 2-bit transmission phase are fully employed to construct a TA antenna. A schematic diagram of the TA antenna is shown in Fig. 3 (a). A linearly polarized horn antenna is adopted as the feeding source, where the operating frequency ranges from 22 to 40 GHz. The polarization of the feeding source is *y*-polarized as illustrated in Fig. 3(a). Since the proposed TA antenna features with wide bandwidth, the spillover and illumination efficiencies should be considered at different frequencies. After extensive simulations and optimizations, F and D are selected as 70 mm and 85 mm, respectively, leading to an F/D ratio of 0.823. The transmit-panel with the size of 85 mm×85 mm is constructed by 34×34 proposed elements in *x*- and *y*-directions. Once F and D are determined, the phase distributions on the plane of the transmit-panel are obtained and plotted in Fig. 3(b). Based on the phase distributions, the transmit-panel is configured with the proposed two elements accordingly, and the full TA antenna is simulated. The proposed transmitarray antenna is then fabricated and measured. The realized gain of the proposed TA antenna is measured and presented in Fig. 4, where the simulated counterpart is also plotted for comparison. It is observed that the measured results agree very well with the simulated ones. Based on the measured realized gain, the 1- and 3-dB gain bandwidths are calculated, revealing a fractional bandwidth of 29% and

43.7%, respectively. The aperture efficiency is also calculated with the measured realized gain. As seen in Fig. 4, the proposed TA antenna can reach a peak aperture efficiency of 44.7% at 30 GHz with the realized gain of 26.1 dBi. The aperture efficiency is above 40.0% from 27 to 32 GHz with a fractional bandwidth of 16.9%.

III. Mthod to Enhance the Bandwidth of Lens Antenna Based on Dielectric Stubs

In the design of transmitarray antennas, the spherical waves radiating from the feed source will impinge on the phase-shifting surfaces. It should be noted here that all elements are not always illuminated with normal incidence waves, and elements at different positions within the phase-shifting surfaces are sometimes illuminated with different oblique incident angles and polarizations as can be seen in Fig. 5(a). Moreover, the same element at different positions within the phase-shifting surfaces could also demonstrate distinguished frequency responses due to the effects of oblique incidence on elements. If we do not consider the oblique incidence effects and only compensate for the phase shift of each element based on the frequency response under normal incidence, the performance of the corresponding TA would be degraded as the phase error introduced by oblique incidence effects is significant. In order to diminish the aforementioned oblique incidence effects, it is critical to obtain the actual phase response of each element in which all oblique incidence effects are taken into account. Most of the works in the literature focus on the unit cell simulation with PBCs [14][15], where every incident angles and two polarizations shoubd all be simulated (TE and TM modes in two principal planes, and mixed TE and TM modes at other planes). Moreover, as incident angles increase, higher Floquet modes must be added to obtain accurate frequency responses, which makes the unit cell simulation even slower. To accelerate the design, we then construct element arrays (EAs) that consist of identical elements and simulate them in the real array enviroment to monitor the phases on two well-defined observation planes. The actual phase response of each specific element at different positions of the EA can then be extracted by subtracting the phases on the observation planes. Specifically speaking, as illustrated in Fig. 5(a), the incident reference plane is P_0 and the outgoing reference plane is P_1 which are planes on or close to the two surfaces of the phase-shifting surfaces. In the case of phase tunning elements with varying height, the two reference planes are the top and bottom surface planes of the highest element as shown in Fig.5 (b), which is identical to the reference port plane in unit cell simulation with PBCs. The actual phase shift of each element in the real array environment is the phase difference between the reference planes P_1 and P_0. If the phase-shifting surfaces of a transmitarray antenna are implemented by elements with the phase shift resolution of r(°), the total required amount of phase states is thus $n = 360°/r$. In this case, we need to figure out the actual phase shift of each phase state at different positions in the real array environment, which can be extracted and obtained by simulating the EAs built by elements of each phase state. The extracted actual phase shifts of different elements in a real array environment can then be fully leveraged to implement a transmitarray antenna, expecting to enhance the performance (e.g., higher gain, bandwidth, and higher aperture efficiency, etc.) as the oblique incidence effects are significantly reduced or even removed. Compared to the method of simulating unit cell with PBCs, the proposed one requires much less number of simulation models as well as less simulation time when the phase shift resolution is 180° or 90°, i.e., 1-bit or 2-bit.

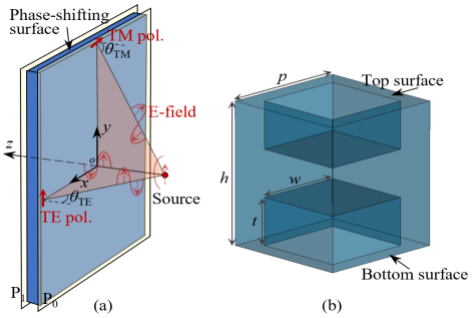

Fig. 5 (a) Configuration of the TA, (b) element for phase tuning.

Four corresponding EAs of these elements are then constructed with a square aperture of 100 mm × 100 mm. The EAs are center fed by a linearly polarized horn antenna at an optimum F/D of 0.37 based on the $\cos^q$ model. As displayed in Fig. 5(a), the co-polarization of the E-field (Ey components) on the incident reference plane (z = 0 mm) and the outgoing reference plane (z = 19.5 mm, i.e., the surface planes of the highest element) are extracted since the feed source is linearly polarized and the phase shifting element does not introduce any mode transformation (S_{21}(TE-TM) < -60 dB and S_{21}(TM-TE) < -60 dB). Otherwise, both Ey- and Ex components should be considered. The actual phase shift of each element at different positions in the real array environment is then calculated at 26 GHz by subtracting the phases of the Ey components on these two reference planes. The actual phase shift (APS) of each element of these four EAs at different positions are then illustrated in Fig. 6, where it is observed that the APSs of elements at the center positions of the EAs are quite similar to the results obtained from a unit cell with PBCs under normal incidence. Nonetheless, as elements locate further away from the center position, a larger phase difference between the EA's and UC's results is observed, which is attributed to the oblique incidence effects. By combining the phases at each position from EAs simulations in Fig. 6, the actual phase curves in a real array environment can be obtained.

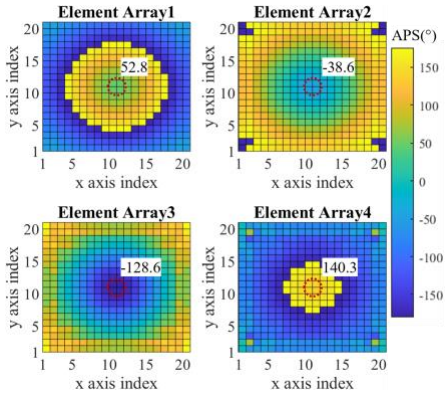

Fig. 6. Extracted actual phase shift values of four designed EAs.

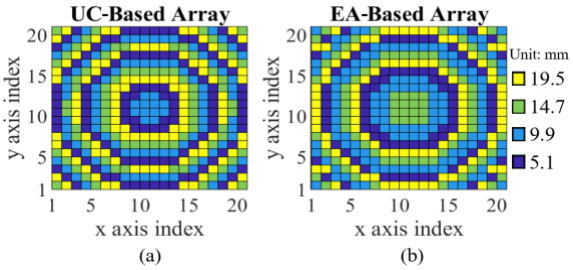

Fig. 7. Configurations of the (a) UC-based TA and (b) EA-based TA.

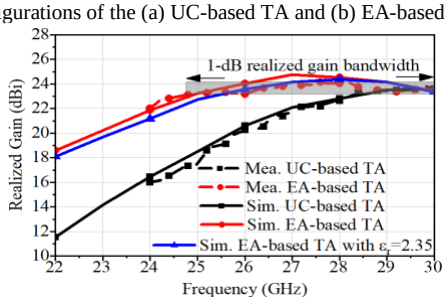

Fig. 8. Comparison of the measured realized gain and simulated ones.

The transmitarray using the actual phase response from EAs' simulation (denoted as EA-based TA) is designed by compensating for the required phase of each element located at position (m, n) in the array with the actual phase curve at position (m, n). Another transmitarray is designed without considering the oblique incidence effects by using the phase response of UC under normal incidence (denoted as UC-based TA) for comparison. Fig. 7 shows the configurations of two transmitarrays of 20 × 20 elements with the same F/D of 0.37. Two prototypes of transmitarrays with 20×20 elements (100 mm × 100 mm) are manufactured using a 3-D printer with the filament of ABS (ε_r = 2.55, tanδ = 0.01), and the fixtures are all made of ABS as well. The measured realized gain agrees well with the simulated ones, as plotted in Fig. 8. A little deviation is observed for the EA-based TA, which owes to the fabrication tolerance of the dielectric lens. When the relative permittivity of the dielectric lens is 2.35, the simulation and measurement results match well. The measured 1-dB bandwidth is 19.2% which is significantly enhanced compared to the UC-based TA.

IV. Conclusion

In this paper, we introduce two efficient methods to enhance the bandwidths of transmitarray antennas: one is for transmitarray antenna based on polarization-rotation structures and the other is for lens antenna based on dielectric stubs. The simulated and measured results agree well with each other, demonstrating the effectiveness of the proposed methods.

References

[1] T. S. Rappaport *et al*., "Millimeter-wave mobile communications for 5G cellular: it will work!" *IEEE Access*, vol. 1, pp. 335-349, May 2013.

[2] C. Dehos, J. L. Gonzslez, A. De Domenico, D. Ktenas, and L. Dussopt, "Millimeter-wave access and backhauling: The solution to the exponential data traffic increase in 5G mobile communications systems?" *IEEE Commun. Mag.*, vol. 52, no. 9, pp. 88-95, Sep. 2014.

[3] A. H. Abdelrahman, A. Z. Elsherbeni, and F. Yang, "High-gain and broadband transmitarray antenna using triple-layer spiral dipole elements," *IEEE Antennas Wireless Propag Lett*., vol. 13, pp. 1288-1291, 2014.

[4] S. Tuloti, P. Rezaei, and F. Hamedani, "High-efficient wideband transmitarray antenna," *IEEE Antennas Wireless Propag Lett*., vol. 17, no. 5, pp. 817-820, May. 2018.

[5] G. Liu, H. Wang, J. Jiang, F. Xue, and M. Yi, "A high-efficiency transmitarray antenna using double split ring slot elements," *IEEE Antennas Wireless Propag Lett*., vol. 14, pp. 1415-1418, 2015.

[6] P. Mei, S. Zhang, X. Q. Lin, and G. F. Pedersen, "A millimeter-wave gain-filtering transmitarray antenna design using a hybrid lens," *IEEE Antennas Wireless Propag Lett*., vol. 18, no. 7, pp. 1362-1365, July 2019.

[7] Y. Cai, W. Li, K. Li, S. Gao, Y. Yin, L. Zhao, and W. Hu, "A novel ultrawideband transmitarray design using tightly coupled dipole elements," *IEEE Trans. Antennas Propag*., vol. 67, no. 1, pp. 242-250, Jan. 2019.

[8] A. Abdelrahman, P. Nayeri, A. Elsherbeni, and F. Yang, "Bandwidth improvement methods of transmitarray antennas," *IEEE Trans. Antennas Propag*., vol. 63, no. 7, pp. 2946-2954, Jul. 2015.

[9] P. Feng, S. Qu, and S. Yang, "Octave bandwidth transmitarrays with a flat gain," *IEEE Trans. Antennas Propag*., vol. 66, no. 10, pp. 5231-5238, Oct. 2018.

[10] Y. Ge, C. Lin, and Y. Liu, "Broadband folded transmitarray antenna based on an ultrathin transmission polarizer," *IEEE Trans. Antennas Propag*., vol. 66, no. 11, pp. 5974-5981, Aug. 2018.

[11] K. Mavrakakis, H. Luyen, J. Booske, and N. Behdad, "Wideband transmitarrays based on polarization-rotating miniaturized-element frequency selective surfaces," *IEEE Trans. Antennas Propag*., vol. 68, no. 3, pp. 2128-2137, Mar 2020.

[12] P. Mei, G. F. Pedersen, and S. Zhang, "A broadband and FSS-based transmitarray antenna for 5G millimeter-wave applications", *IEEE Antennas Wireless Propag Lett*., vol. 20, no. 1, pp. 103-107, 2020.

[13] Y. Cai, P. Mei, X. Q. Lin, and S. Zhang, "A Generalized Method for Gain Bandwidth Enhancement of Transmitarray Antennas Considering Oblique Incidences," *IEEE Transactions on Circuits and Systems II: Express Briefs*, pp. 1–1, 2023, doi: 10.1109/TCSII.2023.3297393.

[14] G. B. Wu, S. W. Qu, C. Ma, S. Yang, and C. H. Chan, "Reflectarray antenna design with arbitrary incident and reflection beam angle," *IEEE Trans. Antennas Propag.*, vol. 66, no. 11, pp. 5964–5973, Nov. 2018.

[15] E. R. F. Almajali and D. A. McNamara, "Angle of Incidence Effects in Reflectarray Antenna Design: Making gain increases possible by including incidence angle effects," *IEEE Antennas Propag. Mag.*, vol. 58, no. 5, pp. 52–64, Oct. 2016.